Performance analysis of acceleration effect on paraffin melting in finned copper foam

Jincheng Tang[a], Yongqi Xie[a,*], Shinan Chang[a], Zhenrong Yan[b,**], Hongwei Wu[c], Hongxing Zhang[d]

[a]School of Aeronautic Science and Engineering, Beihang University, Beijing, 100191, China
[b]School of Mechanical and Automotive Engineering, Shanghai University of Engineering Science, Shanghai 201620, China
[c]School of Physics, Engineering and Computer Science, University of Hertfordshire, AL10 9AB, UK
[d]Beijing Key Laboratory of Space Thermal Control Technology, China Academy of Space Technology, Beijing 100094, China

*Corresponding author: Tel: +86(10) 8233 8081, Fax.: +86(10) 8233 8952, E-mail: xyq@buaa.edu.cn
**Corresponding author: Tel: +86(10) 2167791492, E-mail: yanzr2010@163.com

Abstract

Phase change material (PCM) has great potential in thermal control of aircraft electronic components because of their excellent latent heat capacity. In the current work, a finned copper foam phase change energy storage unit (PCESU) was fabricated using n-eicosane, 97.2% porosity copper foam and 0.8 mm fins. The effects of four different heating power i.e. 40 W, 45 W, 50 W, 55 W corresponding to heat flux of 0.4 W/cm^2, 0.45 W/cm^2, 0.5 W/cm^2, 0.55 W/cm^2 at four different centrifugal acceleration magnitudes, i.e. 0 g, 5 g, 9 g, 13 g with three different acceleration directions on the thermal performance of PCESU were experimentally studied in a systematic manner. Experimental results indicated that: (1) the acceleration direction has a significant effect on the thermal performance of PCESU which can be improved for the cases of vertical and opposite direction, whereas restrained for the case of same direction. Under acceleration condition, the average melting time for the cases of opposite and same direction are 15.19% and 37.10% longer than that for the case of same direction, respectively. The temperature difference of PCESU while the melting is completed is 95.12% higher than that for the case of vertical direction on average. (2) the effect of acceleration magnitude on the heat transfer performance can be determined significantly when the acceleration direction is applied. The melting time decreases with the increase of the acceleration magnitude along vertical direction and increases along the same direction. The temperature difference decreases with the increase of the acceleration magnitude along vertical direction, whereas increases along opposite or same direction. Moreover, the melting time and temperature difference for acceleration magnitude changing from 0 g to 5 g have an obvious larger change rate than that from 5 g to 9 g and 9 g to13 g. (3) the melting time is negatively correlated to the heating power, whereas the temperature difference is positively correlated to the heating power. The proposed two-dimensional (2D) simplified model can be helpful to reveal the physical mechanism of the thermal performance of PCESU.

Keywords: Phase change energy storage; centrifugal acceleration; thermal performance; finned metal foam; phase change material

Nomenclature

Abbreviation

ETC	effective thermal conductivity
FMF	finned metal foam
PCESU	phase change energy storage unit
PCM	phase change material
PMS	porous metal structure

Symbols

$\vec{a}$	the acceleration vector ($s \cdot m^{-2}$)
A	additional source to damp the velocity in solid PCM
C_f	form drag coefficient
f_1	liquid fraction
k_{ef}	effective thermal conductivity of the PCM/foam composite ($W \cdot m^{-1} \cdot K^{-1}$)
K	permeability
q	heat flux ($W \cdot m^{-2}$)
t_m	the complete melting time of n-eicosane (s)
t_m-v, t_m-o, t_m-s	t_m in vertical, opposite and same acceleration direction (s)
△T	the temperature difference of PCESU when the melting is just completed (℃)
△T-v,△T-o, △T-s	△T in vertical, opposite and same acceleration direction (℃)
T_m, T_{m1}, T_{m2}	The melting temperature, lower and upper limits of the melting temperature of paraffin (K)

Greek symbol

δ	liquid fraction of PCM in the porous medium
ε	the porosity of metal foam
λ	Thermal conductivity ($W \cdot m^{-1} \cdot K^{-1}$)
μ	viscosity ($N \cdot s \cdot m^{-2}$)
ρ	density ($kg \cdot m^{-3}$)

Subscripts

f	phase change material
s	copper foam

1. Introduction

Over the past two decades, high-power electronic components for intermittent operation on aircraft are increasing remarkably with the rapid development of hypersonic vehicles, rockets, airborne laser weapons and radar. With a power level ranging from 0 W/cm^2 to 30 W/cm^2, the heat generation of these components is usually local, variable and short-term change that brings a severe problem for temperature control of thermal management system. It is recognized that phase change material (PCM) could be used to solve this problem due to their stable chemical property, excellent reusability, low cost and high enthalpy [1-3].

PCM have been widely used in different area such as building heat storage, solar energy utilization, thermal management of electronic components [4]. Among various PCMs, paraffin is considered as a classical PCM with its excellent physical performance that can be applied to heat sinks and passive thermal management systems [5,6]. However, poor thermal conductivity of paraffin becomes the bottleneck of its practical applications. It is known that the thermal property of PCM would be greatly enhanced by adding highly porous metal foam. Many investigations on enhancing the thermal properties of PCM have been carried out over the past years. It is indicated that the metal foam could significantly enhance the thermal performance of PCM [7-15]. Effective thermal conductivity (ETC) is recognized as an important parameter to evaluate the reinforcing effect of foam metal on PCM. Yao et al. [16] proposed a new model to calculate the ETC of high porosity open-cell metal foams. Compared with available experimental data, the average deviation of the predicted model was within 10%, which showed better results than other reported ETC models. Bai et al. [17] performed an analytical study to estimate the individual components of the effective thermal conductivity in fluid-saturated metal frame and prismatic cellular structures. It was found that their predicted results agreed well with existing experimental data and those obtained from exhaustive numerical computations.

In addition to metal foam, the thermal conductivity of PCM can also be significantly improved by adding fins. By adding aluminum fins with circular and square cross-sectional area into n-eicosane, the enhancement effect of fins on PCM performance was experimentally studied by Ashraf et al. [18]. Their results demonstrated that the latent heat could be the major factor effecting the thermal properties of PCM. Wang et al. [19] experimentally investigated the thermal performance of cylindrical battery with finned paraffin. They concluded that the thermal resistance could change significantly with the thermal structure and the thermal performance can be enhanced by using the composite PCM with finned structure. Hussein et al. [20] conducted an experimental study to investigate the effect of finned pipes and metallic strips on the thermal property of solar water heaters with PCM. Their results showed that, compared with that of unfinned pipes, the energy utilization of molten wax with finned pipes and copper strips could be increased by 47% and 304%, respectively. Ali et al. [21] studied the thermal behavior of PCM embedded 2-mm square fin and 3-mm circular fin for passive cooling of electronic devices. Filled with n-eicosane and different number of fins, the thermal property of latent heat storage units were compared. It was found that the 3-mm circular fin combined with PCM presented the optimum enhancement compared with other fins. Ping et al. [22] applied a novel PCM with fin structure to the thermal control of battery. Their results suggested that the PCM-fin structure could maintain the battery surface under a suitable temperature. In general, many studies have concluded that the thermal performance of PCM could be greatly improved by adding fins and copper foam. The finned metal foam (FMF) structure has now become an important method to enhance the thermal property of PCM.

Recently, Qureshi et al. [23] presented a detailed review focused on the enhancement of thermal conductivity by the introduction of highly thermally conductive metallic and carbon-based nanoparticles, metallic foams, expanded graphite and encapsulation of PCM. It was stated that this review will be helpful to explore and develop better materials and techniques so that PCMs can be used with much better performance. A novel microchannel heat sink including PCM, pin-fins and carbon nanotube was experimentally studied by Xu et al. [24]. With the Graphene oxide particles nanofluids pulsating flow, their study showed that the thermal performance of PCM was obviously enhanced. Using expanded graphite as the thermal conductivity enhancer, Zhang et al. [25] prepared a composite PCM by adding nano-SiO_2 to n-eicosane. Their results demonstrated that the

composite PCM had excellent application in thermal management. It is also noted that high thermal performance nanoparticles have been widely used to enhance the ETC of PCM [26-29]. Moreover, Ramakrishnan et al. [30] experimentally studied the feasibility of integrating form-stable PCM composites into cementitious composites. It was found that the composite PCM having contact angle higher than 90^{o} and negative wetting tension properties successfully prevented the PCM leakage in cementitious composites due to counter-water affinity properties. Chamkha et al. [31] investigated the composite heat sink of PCM and metal foam under pulse heating conditions. They found that the cooling rate of the element can be increased by PCM-heatsink when the heat pulse was activated. Hu et al. [32] performed a combined experimental and numerical study on the heat transfer performance of PCM in a cubic cell porous metal structure (PMS). The numerical results were in good agreement with experimental results, which indicated that heat transfer characteristics can be predicted using pore-scale numerical simulation. It was also found that the temperature field of PCM with PMS was more uniform and heat transfer mechanics was different for PCM with and without PMS. Zhang et al. [33] experimentally studied the effect of centrifugal acceleration on paraffin melting in high porosity copper foam. The solid-liquid interface and temperature distribution of the composite PCMs were obtained. They stated that the centrifugal acceleration had a significant effect on the melting process of PCM. The convection and heat transfer coefficient of liquid paraffin was gradually enhanced with the increase of the centrifugal acceleration. However, the effect of acceleration direction was not taken into account. Under rotating conditions, Yang et al. [34] numerically studied the heat transfer process in metal foam and established a correlation for predicting interstitial heat transfer Nusselt number. The correlation results showed a good validity within the studied range of corresponding parameters. Wu et al. [35] numerically investigated the effects of vibration frequency and orientation of the vibration axis on melting processes. It was observed that for low frequency mechanical vibration, the enhanced mixing of molten phase change materials (PCMs) would accelerate the melting processes critically. While for a higher vibration frequency could lead to an obviously faster charging speed. When the vibration axis is parallel to the gravity, the thermal response rate was the fastest.

It appears from the previous investigations that the FMF structure can be an effective method to enhance the ETC of PCM. However, most of the work is conducted under the normal ground environment. To the best of the authors' knowledge, there is a lack of in-depth experimental investigation on the thermal performance of composite PCM with FMF structure under acceleration condition. Moreover, no research is implemented to study the effect of acceleration direction on the paraffin melting. To this end, the objective of current work is to present the results attained through acceleration simulation experiment for PCESU based on finned copper foam and paraffin. The effects of several control parameters such as different centrifugal accelerations, acceleration directions and heating power on the thermal performance of PCESU are discussed in a systematic manner.

2. Experimental apparatus and method

2.1. Experimental apparatus

2.1.1. Experimental system

In the current work, the experimental investigation was implemented at the Reliability and Environmental Engineering Laboratory at Beihang University, Beijing, China. The experimental system mainly consists of acceleration and control subsystem, test section, and data acquisition subsystem. The schematic diagram of the experimental test rig is shown in Fig. 1.

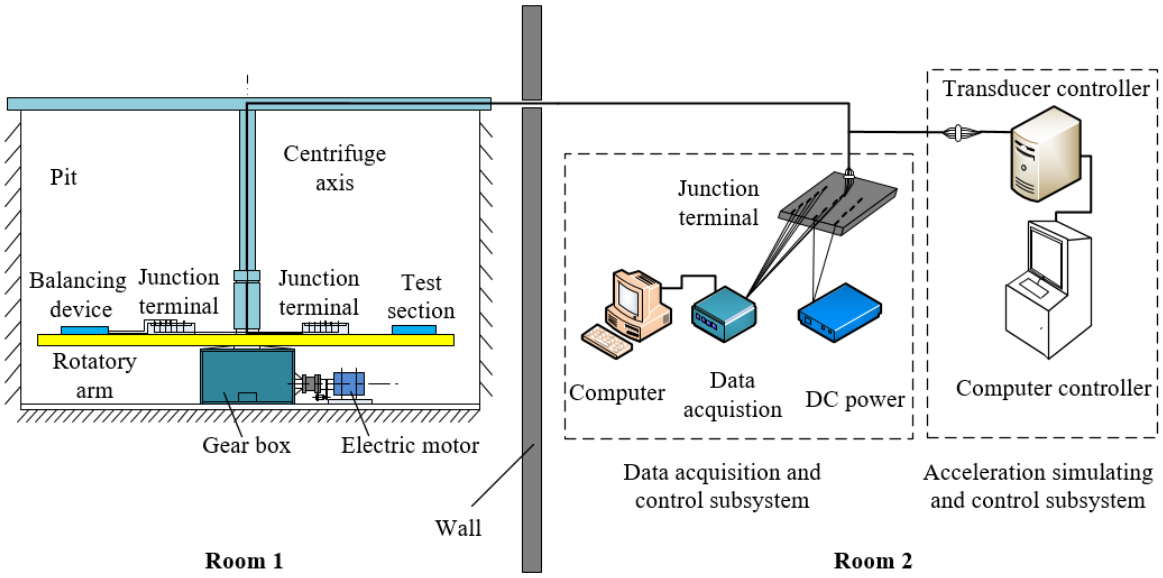

Fig. 1. Experimental test system.

The centrifuge and acceleration simulating and control subsystem are set up in two separate rooms. The required acceleration magnitude was controlled by an acceleration simulation and control subsystem and generated by centrifuge Y 53100-3/Z F. The motor of centrifuge was three-phase asynchronous motor and the rotatory arm was driven through a gear box. As shown in Fig. 1, the centrifuge was installed in room 1 and was controlled by the acceleration simulating and control subsystem in room 2. Fig. 2 is a photo of the test component along the rotatory arm. During the test, the test section was setup in a fixed box at the end of the rotatory arm with maximum acceleration magnitude up to 13g. The experiment was carried out according to the GB/T 2424.15 standard.

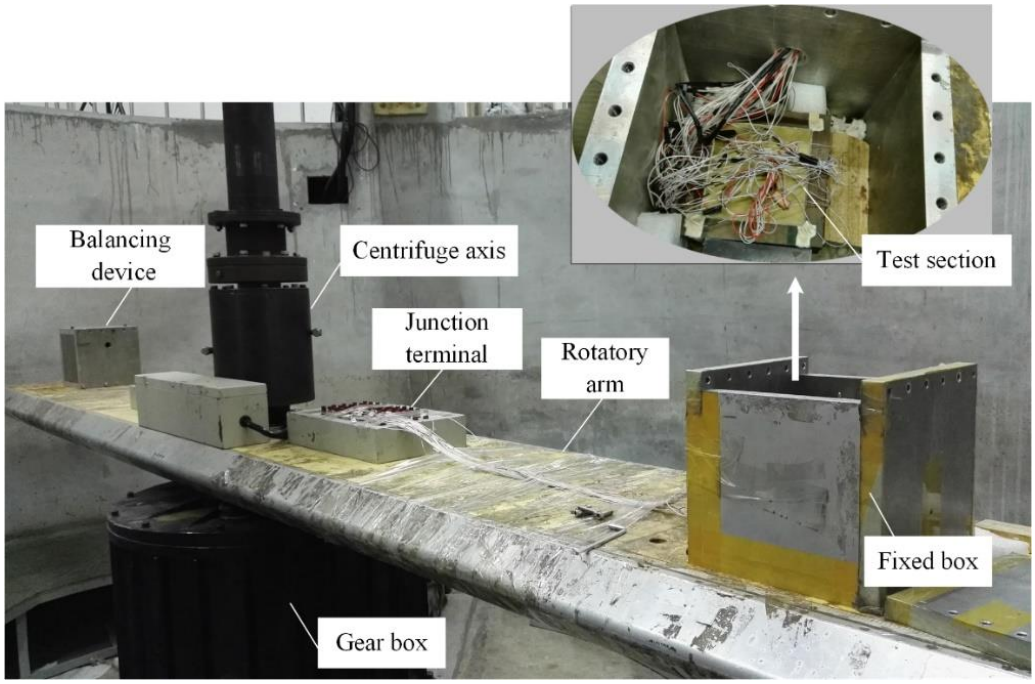

Fig. 2. The photo of test section in rotation arm.

Data acquisition and control subsystem mainly consisted of three HP 34901A plug-in modules and an Agilent 34970A multi-functional data acquisition instrument which can collect and record data such as current, resistance, voltage, and temperature. The power supply was DH 1722A-2 DC voltage and current stabilized power supply, which can automatically measure its output current, directly read and calculate the heating power.

2.1.2. PCESU design

The composite structure of FMF and paraffin has become an effective approach to enhance the ETC of PCM and it has a greater ETC than the composite structure with foam and paraffin only. In the present study, a finned copper foam PCESU was designed and fabricated. The copper foam of PCESU was nickel-plated copper foam with 97.2% porosity with pore size of 25 PPI. With excellent latent heat capacity and the melting point 36.8 ~38.5 ℃, n-eicosane can keep the electronic components in an optimum working temperature range (-10 ℃ ~ 50 ℃) during melting process. In addition, since its melting temperature was close to the ambient temperature, the n-eicosane with a purity of 98% (Aladdin, https://www.aladdin-e.com/zh_en/) was used as phase change material that was beneficial to reduce the heat loss.

As shown in Fig. 3, the PCESU was made up of core body and wallboards. The slab of copper foam was customized from a copper foam manufacturer (YiYang Foametal New Material Co. Ltd). The copper foam was first cut into 100.0 mm ×100.0 mm ×25.0 mm flat rectangular body and then the fins were inserted into it to form a finned copper foam with interference fit. The fin thickness was 0.8 mm and the distance between the fins was 12.5 mm. In order to reduce the thermal resistance, the heat conductive adhesive is coated on the surface of fins. The core body was a "sandwich" structure consisting of two copper plates and a copper foam. In addition, in order to prevent dead corner during paraffin injection, length of the fins was designed to be 75 mm (less than the size of the core), and the fins were staggered to make the core structure symmetrical that can lead to a more uniform heat transfer in PCESU. The size of the whole "sandwich" core body was 100.0 mm × 100.0 mm × 35.0 mm.

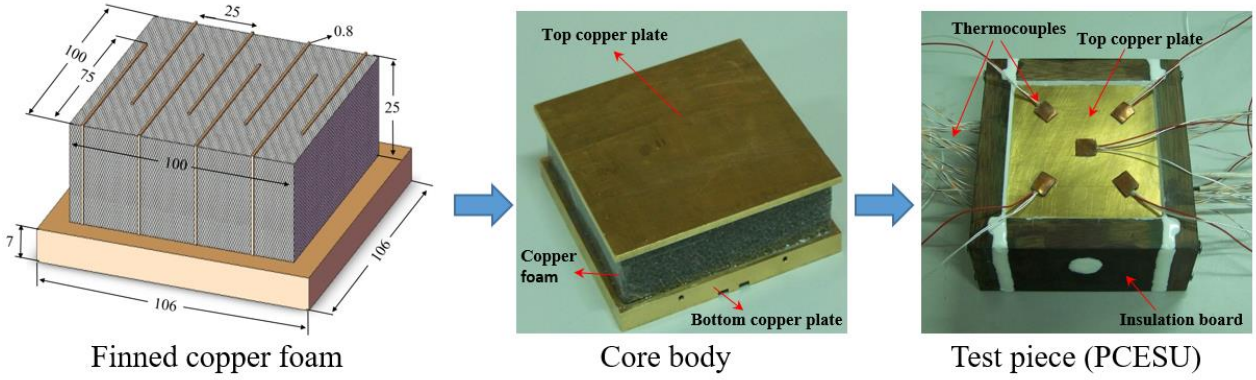

Fig. 3. Structure and assembly process of PCESU.

The fins were welded to the top copper plate of 106 mm × 106 mm × 3 mm and the bottom copper plate of 106 mm × 106 mm × 7 mm that can reduce the contact thermal resistance with low temperature brazing process. In order to decrease the thermal resistance, the thickness of the copper base plate was designed to be thicker than the top plate. An electronic-heating plate (100 mm × 100 mm) was embedded in the bottom plate. Through the design of combining electronic-heating plate with shell, the heat loss between the heat source and test section was minimized.

The phenolic resin insulation board with thermal conductivity less than 0.02 W/(m·K) was used to attach the wallboards around the test section, which can greatly reduce the heat loss along the wallboards. This will make sure that the heat can be only transferred and absorbed by PCESU. After completing the shell packaging of PCESU, the paraffin was filled through vacuuming method. In the current work, the vacuum degree in the shell was less than 0.1 Pa prior to filling the paraffin. This can make the PCM is fully and uniformly filled into the test section. The physical properties of the materials used in the current experiment were illustrated in Table 1.

Table 1 Physical properties of the materials of PCESU.

Materials	Parameters	Value
n-eicosane	Density（kg/ m³）	778
	Melting temperature（℃）	36.8~38.5
	Specific heat capacity（J/(kg· k)）	2082
	Thermal conductivity(W/(m· k))	0.27
	Latent heat（J/kg）	241000
Copper foam	Porosity (%)	97.2
	Density（kg/ m³）	8930
	Specific heat capacity（J/(kg· k)）	386
	Thermal conductivity (W/(m· k))	398
Copper plate	Density（kg/ m³）	8440
	Specific heat capacity（J/(kg· k)）	377
	Thermal conductivity (W/(m· k))	109
Phenolic resin	Thermal conductivity (W/(m· k))	≤ 0.02

Before the melted n-eicosane was poured into the PCESU, a vacuum paraffin fusion irrigation system was firstly used to evacuate the test section and then poured the n-eicosane into it. This method can reduce the remaining gas in the copper foam due to the viscosity of n-eicosane. In addition, the paraffin would produce high expansion stress during the melting process. In order to prevent this stress, the temperature control module was used to keep the temperature of the whole paraffin melting system maintained at approximate 55 ℃ during the pouring process. After pouring, it needs to be sealed and only a little vacuum space may be exist within the test section after cooling.

2.1.3. Temperature measuring points

Fig. 4 shows the arrangement of the temperature measuring points at five different layers within the PCESU. When the test section was heated, the heat flux flowed into the core body from the bottom plate, that was, from layer E to layer A. As can be seen in Fig. 4(a), the distances between the electronic-heating plate and layer E, as well as the distances between different layers were 4 mm, 9 mm, 6.5 m, 6.5 m and 9 mm, respectively. In each layer plane, five temperature measuring points were evenly distributed. A total of twenty five temperature measuring points were allocated in the test section. In layer A, five patch Pt100 temperature sensors were used, while in layers B, C, D and E, twenty probe thermocouples were adopted. In the current experiment, the average temperature of five points in each layer was taken as the temperature of this layer.

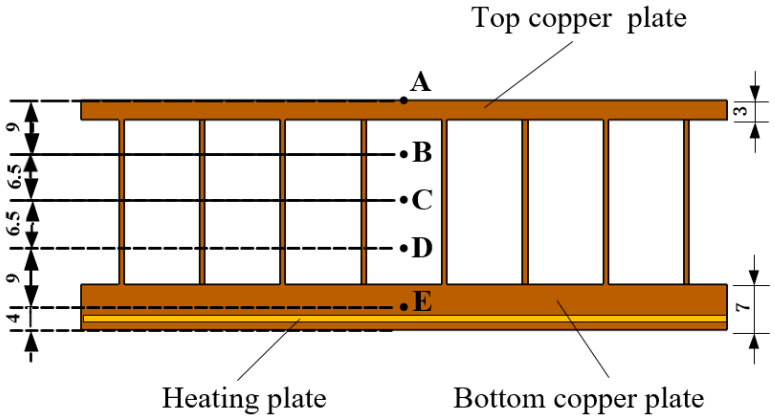

（a）

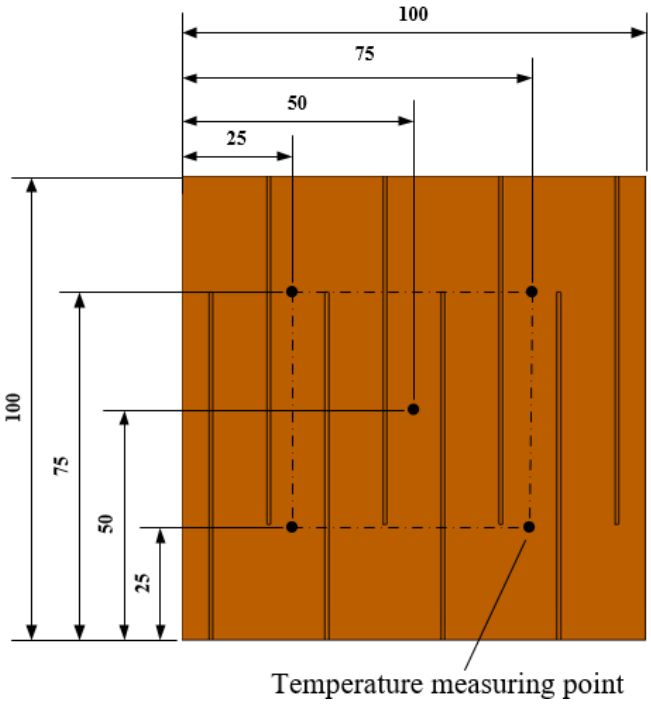

(b)

Fig. 4. The arrangement of temperature measuring points: (a) five layers divided in the PCESU and (b) the position of temperature measuring points in every layer.

2.2. Experimental procedure

The main contribution of the current work is to investigate the effect of acceleration on the thermal performance of PCESU. In the current study, the effects of different heating power, centrifugal acceleration magnitudes and acceleration directions on the melting process of PCESU were studied. Three different control parameters such as heating power, acceleration magnitude and direction, were selected as experimental variables, as illustrated in Table 2. The corresponding heat flux of different heating power were 0.4 W/cm^2, 0.45 W/cm^2, 0.5 W/cm^2 and 0.55 W/cm^2. Three different acceleration directions can be achieved by changing the relative direction of the heat flux and centrifuge acceleration through different placement methods (see Fig. 5) of the test section. For the case of vertical direction, as shown in

Fig. 5(a), the heat flux direction was vertical to the acceleration direction. Similarly, for the case of opposite direction, as illustrated in

Fig. 5(b), the heat flux direction was opposite to the acceleration direction. While for the case of the same direction (see

Fig. 5(c)), the heat flux direction was the same as the acceleration direction. The acceleration magnitude of 0 g means it was under the ground operating conditions. Since the behaviour in opposite and same direction under the ground condition were same for test section, thus, only the results for opposite direction was analyzed at 0 g.

Table 2 Experiment cases setup.

Variables	Value			
Heating power	40 W	45 W	50 W	55 W
Acceleration magnitude	0 g	5 g	9 g	13 g
Acceleration Direction	vertical	opposite	same	

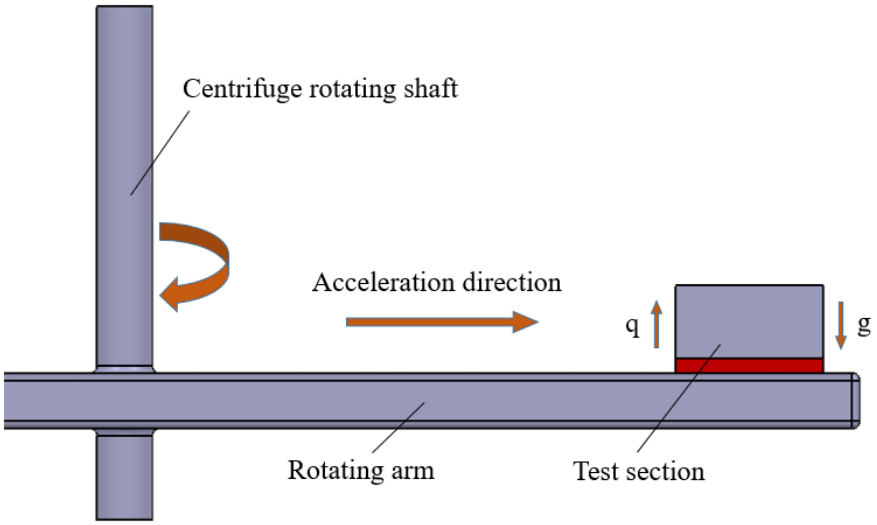

(a) “vertical” direction

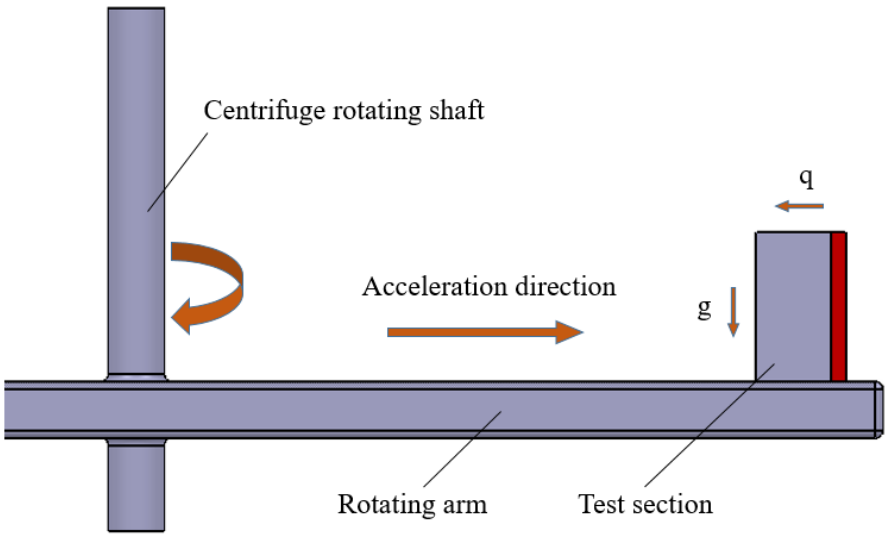

(b) “opposite” direction

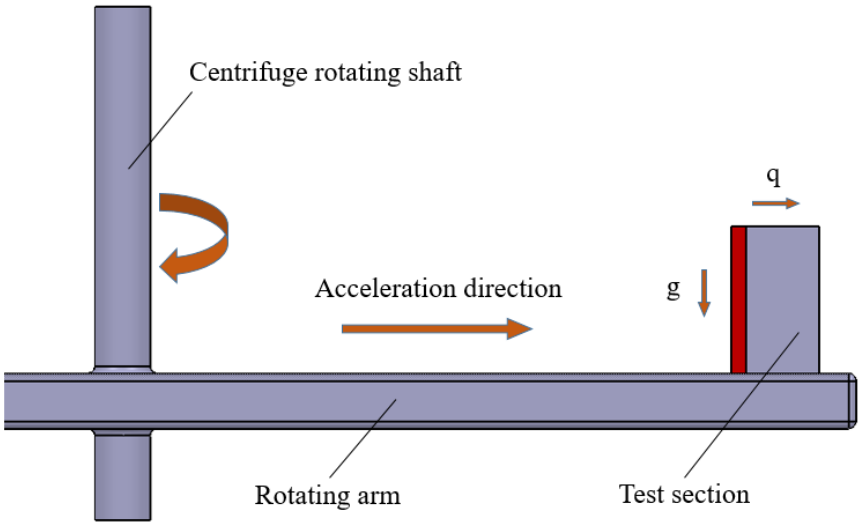

(c) “same” direction

Fig. 5. The test section placement in different acceleration directions: (a) vertical direction (the heat flux direction is vertical to the acceleration direction), (b) opposite direction (the heat flux direction is opposite to the acceleration direction) and (c) same direction (the heat flux direction is the same as the acceleration direction).

2.3. Performance indexes

It should be noted that the melting speed and the inside temperature difference are the most important performance indexes of PCESU. The melting speed of PCESU can be evaluated by the melting time (t_m) of n-eicosane. As shown in Fig. 4, the Layer E was close to the heating source. Once the n-eicosane melted completely, the temperature difference of PCESU can be considered as that between layer E and layer A, represented by ΔT. Therefore, based on the above two thermal performance indexes, the t_m and ΔT of PCESU under different working conditions was obtained. The method to obtain t_m and ΔT was as follows:

When the temperature of layer E reached 36.8 ℃, the corresponding time was t1. When the temperature of layer A was 38.5 ℃, the corresponding time was t2, and the corresponding temperature of layer E was Te. As a consequence, t_m = t2-t1, ΔT=Te-38.5 ℃. For example, the method to get the t_m and ΔT at 40 W and 5 g along vertical direction was demonstrated in Fig. 6. When the temperature of layer E was 36.8 ℃, t1 = 404 s. And when the temperature of layer A was 38.5 ℃, t2 = 1818 s, the corresponding temperature of Layer E was 47.1 ℃, that was, Te = 47.1 ℃. Thus, t_m = 1818 s - 404 s = 1414 s, ΔT = 47.1℃ -38.5 ℃ = 8.6 ℃. In the current study, t_m and ΔT along vertical, opposite and same directions are represented by t_m-v, t_m-o, t_m-s and ΔT-v, ΔT-o, ΔT-s, respectively.

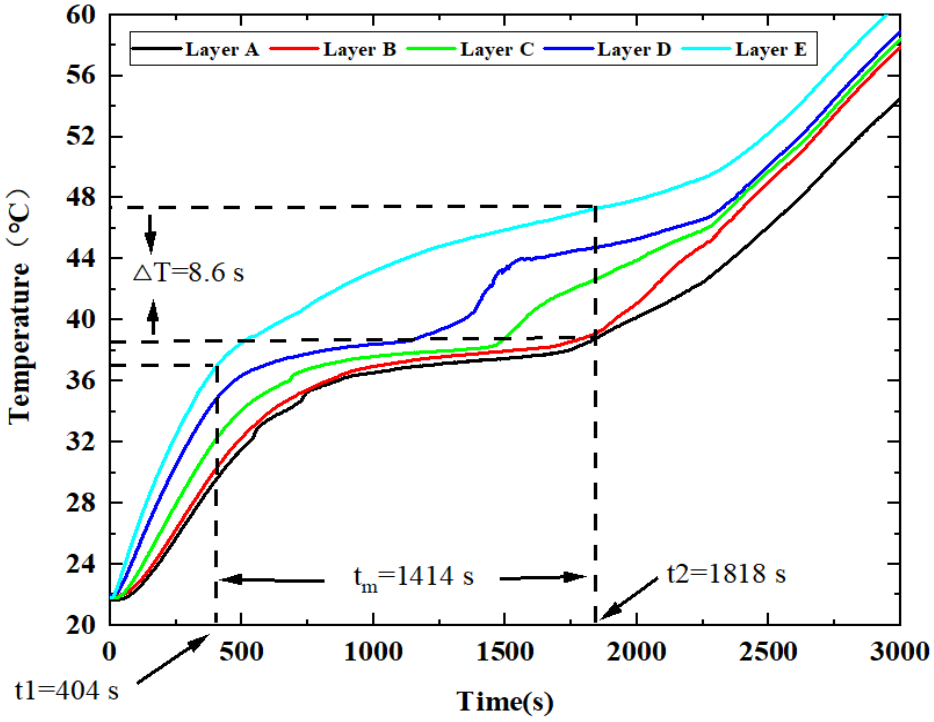

Fig. 6. The method to obtain the t_m and ΔT at 40 W and 5g along vertical direction.

2.4. Experimental uncertainty

In this study, the uncertainties of experimental results mainly included the temperature measurement by thermocouples, dimensions of copper foam, foam porosity, mean heat flux density, t_m and ΔT. The uncertainty of thermocouples relative to standard thermocouple was ±0.3 ℃. The lowest temperature was 21℃, thus the maximum uncertainty of temperature was 1.4%. Similarly, with the minimum size of 0.8 mm, the dimension uncertainties of copper foam was 2.5%. The uncertainty of the copper foam porosity was 0.5%. The uncertainty of the heat flux density was mainly related to the accuracy of voltage *(U)* and current *(I)*. According to the specification data of DH 1722A-2 DC voltage and current stabilized power supply, the uncertainty of *U* and *I* in the current experiment were 0.5% and 1%, respectively. Considering the uncertainty caused by *U* and *I*, as well as caused by heat leakage, the maximum uncertainty of heat flux density was 5%. The errors of t_m and ΔT came from the deviation of reading temperature. Therefore, the lowest temperature was 36.8℃, therefore, the uncertainty of t_m and ΔT were both 0.8%.

3. Numerical approach

In the present study, a 2D model was proposed to investigate the heat transfer performance of PCESU. The following assumptions were made for the purpose of simplification:

(1) The liquid paraffin was considered as incompressible Newtonian fluid, and the density was subjected to the Boussinesq approximation.

(2) The copper foam was assumed to be homogeneous and isotropic, the flow of the liquid paraffin in copper foam was laminar flow, and the volume expansion of the paraffin during phase change was neglected.

(3) The heat transfer of staggered fins is uniform and the heat transfer structure of PCESU can be consider as the combination of some basic units.

As shown in Fig. 7. Computational domain with boundary conditions, a basic unit of PCESU was obtained and the mesh were generated by ICEM CFD commercial software. The enthalpy-porosity model and melting model were used to describe the phase change heat transfer of paraffin. One temperature model was used to explore the heat transfer process with the assumption of local thermal equilibrium. The following governing equations are used to evaluate the flow and heat transfer characteristics of PCM and copper foam.

Continuity equation:

$$\nabla \cdot \left\langle \vec{u} \right\rangle = 0 \tag{1}$$

Momentum equations:

$$\begin{aligned} &\frac{\rho_f}{\delta}\frac{\partial \left\langle \vec{u} \right\rangle}{\partial t} + \frac{\rho_f}{\delta^2}(\left\langle \vec{u} \right\rangle \cdot \nabla)\left\langle \vec{u} \right\rangle = -\nabla \left\langle P \right\rangle^f + \frac{\mu_f}{\delta}\nabla^2 \left\langle \vec{u} \right\rangle \\ &-(\frac{\mu_f}{K} + \frac{\rho_f C_f}{\sqrt{K}}\left|\left\langle \vec{u} \right\rangle\right|)\left\langle \vec{u} \right\rangle + \rho_f \vec{g}\beta(\left\langle T_f \right\rangle - T_m) + \rho_f \vec{a}\beta(\left\langle T_f \right\rangle - T_m) + A\left\langle \vec{u} \right\rangle \end{aligned} \tag{2}$$

where K is the permeability, C_f is the form drag coefficient, and ε is the porosity of metal foam. ρ_f is the density of liquid paraffin. $\vec{a}$ is the acceleration vector. A is an additional source to damp the velocity in solid PCM. δ is the liquid fraction of PCM in the porous medium:

$$\delta = \varepsilon \cdot f_1 \tag{3}$$

f_1 is the liquid fraction which is determined by Eq. (4).

$$f_1 = \begin{cases} 0; T_f \le T_{m1} \\ (T_f - T_{m1})/(T_{m2} - T_{m1}); T_{m1} \le T_f \le T_{m2} \\ 1; T_f \ge T_{m2} \end{cases} \tag{4}$$

where T_f is the temperature of paraffin. T_{m1} and T_{m2} are the lower and upper limits of the melting temperature of paraffin.

Energy equations:

$$\begin{aligned} &(\varepsilon\rho_f c_{pf} + (1-\varepsilon)\rho_s c_{ps})\frac{\partial \left\langle T_f \right\rangle}{\partial t} + \rho_f c_{pf}\left\langle \vec{u} \right\rangle \cdot \nabla \left\langle T_f \right\rangle \\ &= \nabla \cdot (k_{ef} \nabla \left\langle T_f \right\rangle) - \rho_f \varepsilon L \frac{\partial f_1}{\partial t} \end{aligned} \tag{5}$$

where ρ_s is the density of solid paraffin. k_{ef} is the effective thermal conductivity of the PCM/foam composite.

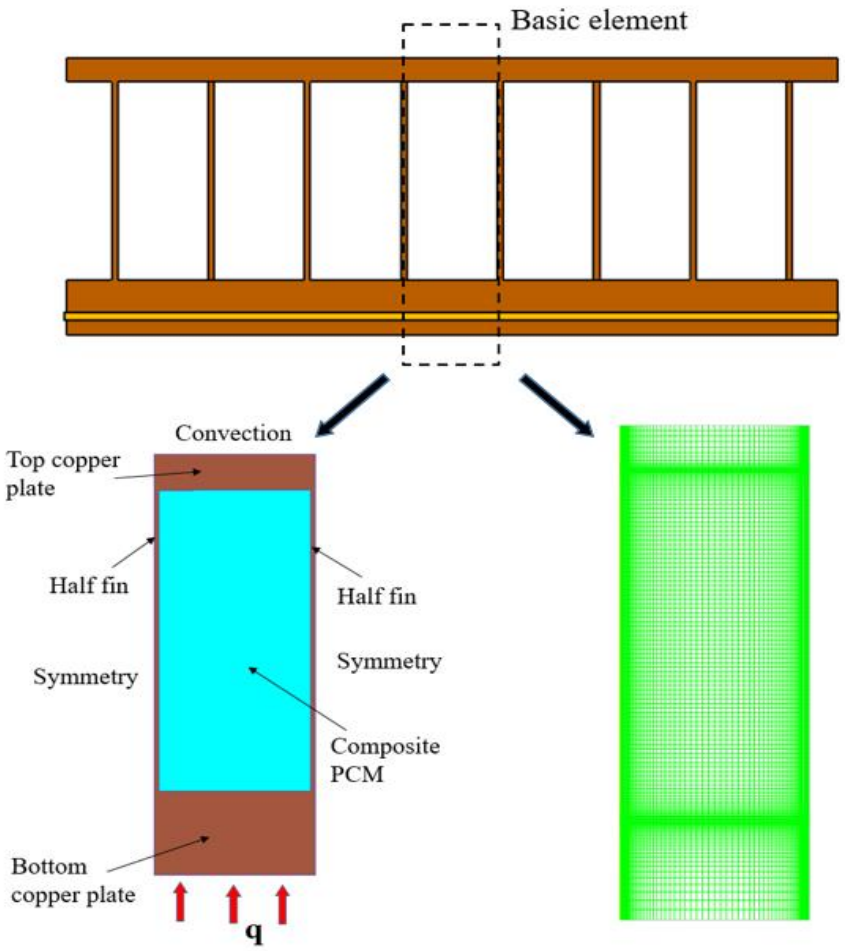

Fig. 7. Computational domain with boundary conditions

The governing equations were solved using finite volume method (FVM) using commercial software ANSYS Fluent 2019R3. The simulation parameters and meshing specifics are given in Table 3. In order to compromise the simulation accuracy and computational time, the mesh independence study with mesh number (7700, 9800 and 11200) and time-step (0.1 s, 0.2 s, 0.5 s and 1s) was analyzed. The permeability and form drag coefficient were calculated according to Ref. [7]. In the present simulation, three different direction were considered (see Fig. 5).

Table 3 Simulation parameters and boundary conditions

Mesh	Quadrilateral elements, Structured mesh, No of Element 9800
Models	Laminar, Melting model, Enthalpy-porosity model
Boundary conditions	Fins: symmetry; Top copper plate: convection; Bottom copper plate: heat flux
Numerical scheme	SIMPLE pressure–velocity coupling was used. Second order accuracy was used.
Convergence criteria	Less the 1e-5
Time step	0.5 s

4. Results and discussion

4.1. Effects of acceleration direction on thermal performance

Fig. 8 shows the temperature changes of Layer A and Layer E with two different heating power of 40 W and 50 W at acceleration magnitude of 5 g under different acceleration direction conditions. From Fig. 8, it can be seen that the acceleration direction has significant effects on the thermal performance of PCESU. The temperature for both layer E and layer A increase rapidly when it is less than 36.8 ℃. When the temperature of layer E reaches about 36.8 ℃, the paraffin begins to melt and there is an inflection point in the temperature curve. Since the layer E is located in the bottom copper plate, its temperature still increases with a slower rate during the melting process. For layer A, its temperature curves are consistent with the curve characteristic of paraffin melting process and the melting process ends when the temperature reaches about 38.5 ℃. In the current work, the temperature curves are consistent with the theoretical melting process of paraffin. In Fig. 8, there are obvious longer t_m-s and bigger ΔT-s than that along other two directions. However, since the curves intersect and are close to each other, it is unclear to compare the performance index between vertical and opposite direction using melting curves of PCESU. In order to compare the effects of acceleration direction on the thermal performance of PCESU more clearly, the t_m and ΔT under different working conditions are obtained using the method described in Fig. 6. Under certain heating power and acceleration, the effects of acceleration direction on the heat performance of PCESU are analyzed by using bar graph.

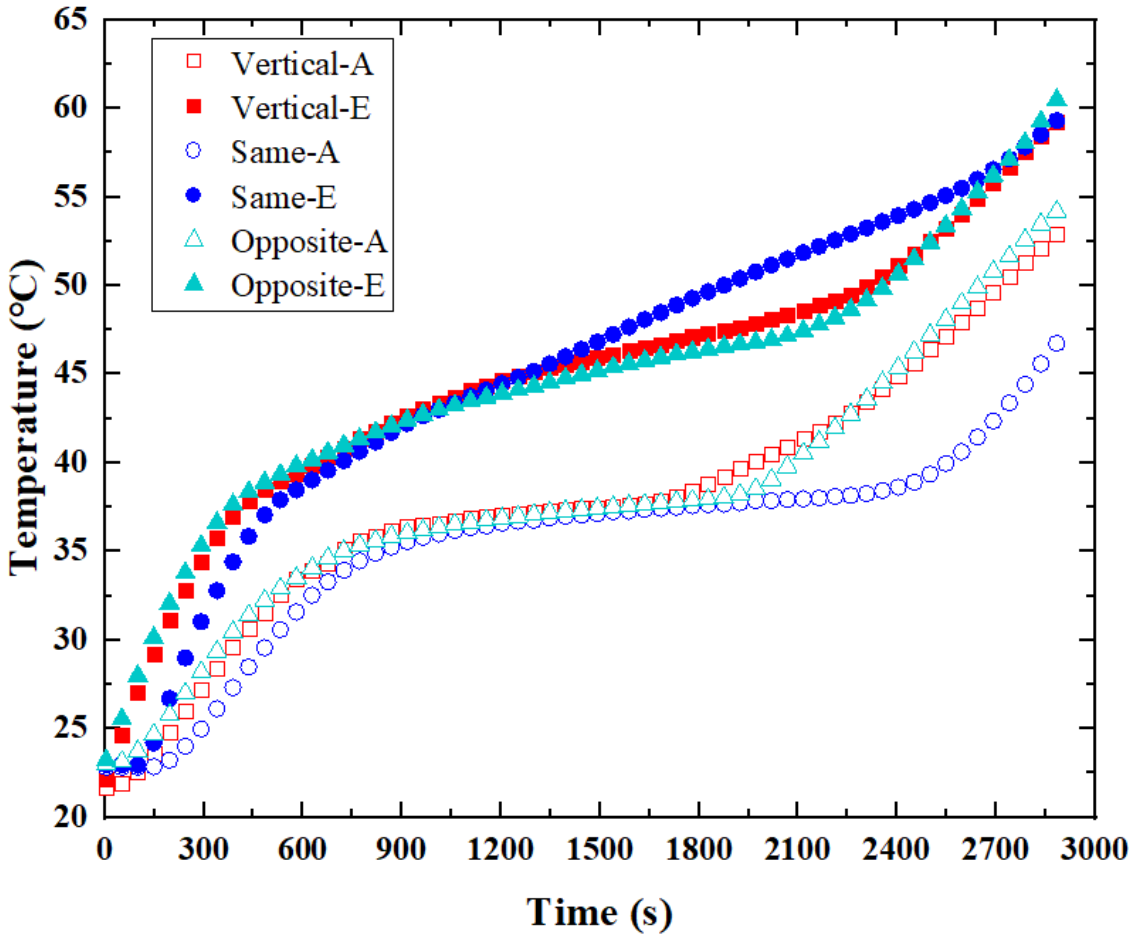

(a) 40 W, 5g

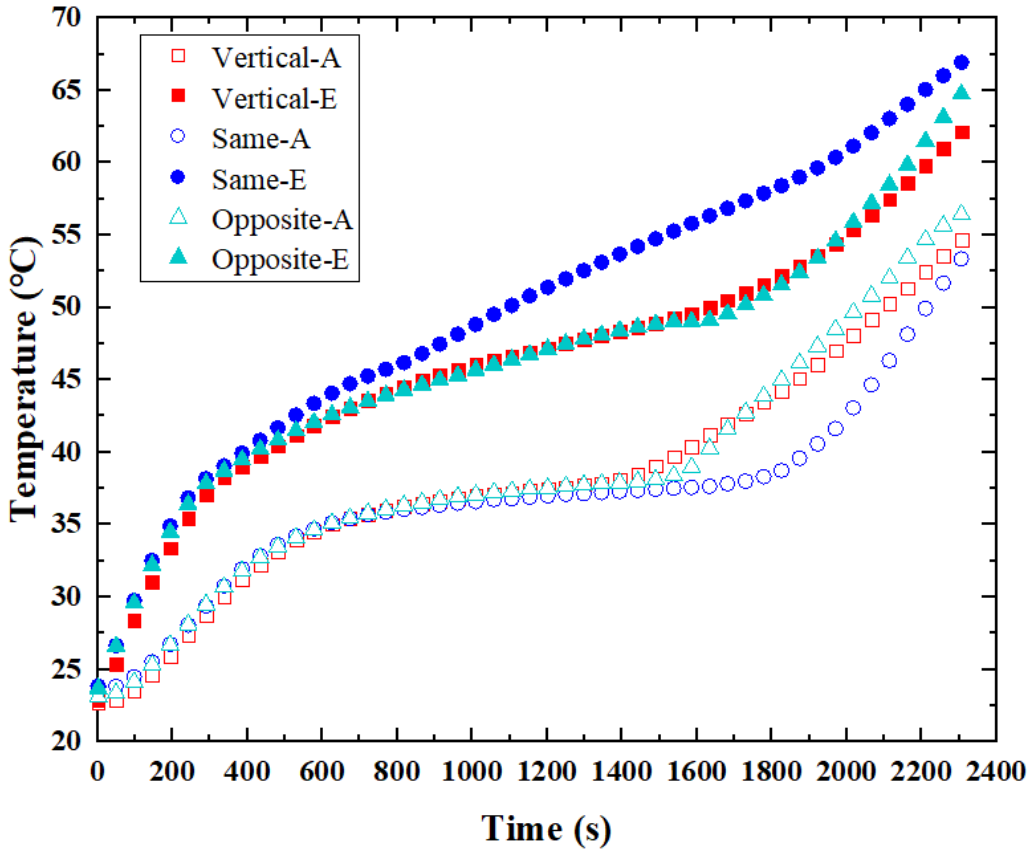

(b) 50 W, 5g

Fig. 8. The effect of acceleration direction: (a) 40 W, 5g and (b) 50 W, 5g.

4.1.1. Effects of acceleration direction on t_m

Fig. 9 demonstrates the effects of acceleration directions on t_m at four different power of 40 W, 45 W, 50 W and 55 W.

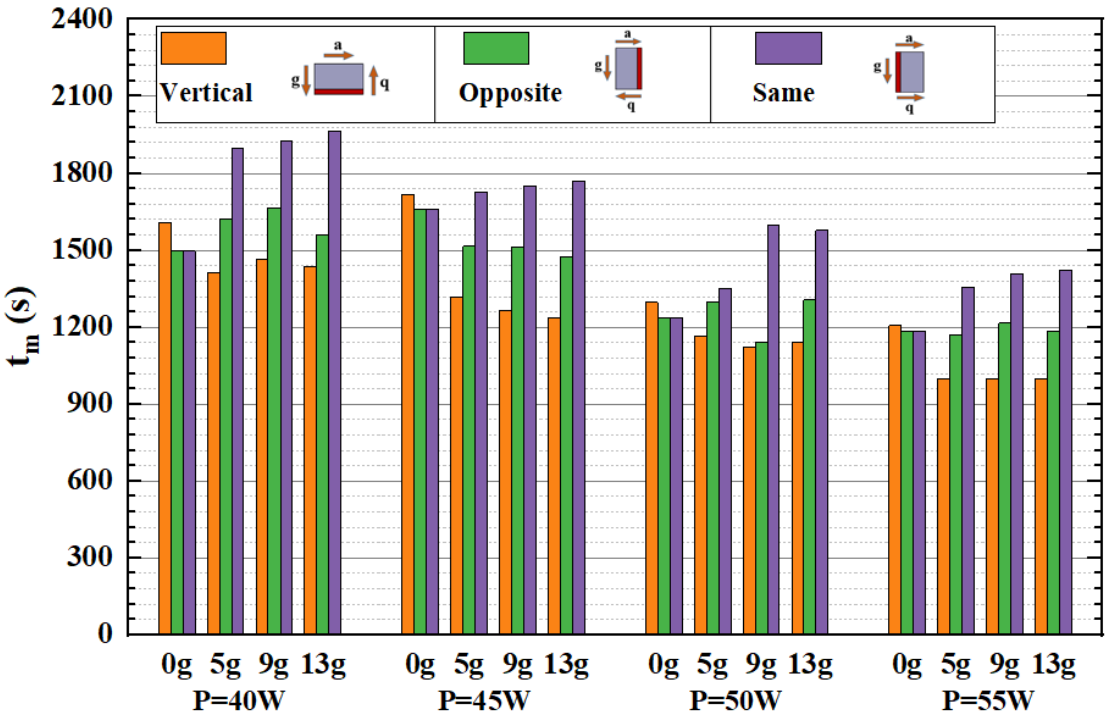

Fig. 9. The effects of acceleration direction on t_m.

It can be seen from Fig. 9 that when the heating power and acceleration magnitude are kept constant, the influence of the acceleration direction on t_m presents a good regularity. With the same heating power and acceleration, t_m-v > t_m-o (or t_m-s) at acceleration of 0 g, while t_m-s> t_m-o > t_m-v under the acceleration environment. For example, at 40 W and 0 g, t_m-v, t_m-o and t_m-s are 1607 s, 1496 s and 1496 s, respectively. And t_m-v is 111 s (7.42%) longer than t_m-o or t_m-s. While at 40 W and 13 g, t_m-v, t_m-o and t_m-s are 1438 s, 1560 s and 1966 s, respectively. And t_m-o and t_m-s are 122 s and 528 s which is longer than t_m-v, with an increase of 8.48 % and 36.72 %, respectively. For all the acceleration operating conditions, the average values of t_m-o and t_m-s are 177 s and 433 s longer than that of t_m-v, with the increase of 15.19% and 37.10%, respectively. That indicates the acceleration direction has obvious effect on the t_m.

4.1.2. Effects of acceleration direction on ΔT

Fig. 10 shows the comparison of ΔT at heating power of 50 W with 5 g along different acceleration directions. When time <300 s, it can be seen from Fig. 10 that ΔT increases rapidly before the paraffin starts to melt and it is kept almost the same along different acceleration directions. Afterwards, ΔT continues to increase gradually followed by a slight decrease. When time >400 s, ΔT-s becomes significantly larger than ΔT-v and ΔT-o, and the ΔT for the latter two are almost the same. When the paraffin is completely melted, ΔT along different acceleration directions begins to decrease gradually and ΔT-s is still larger than ΔT-v and ΔT-o.

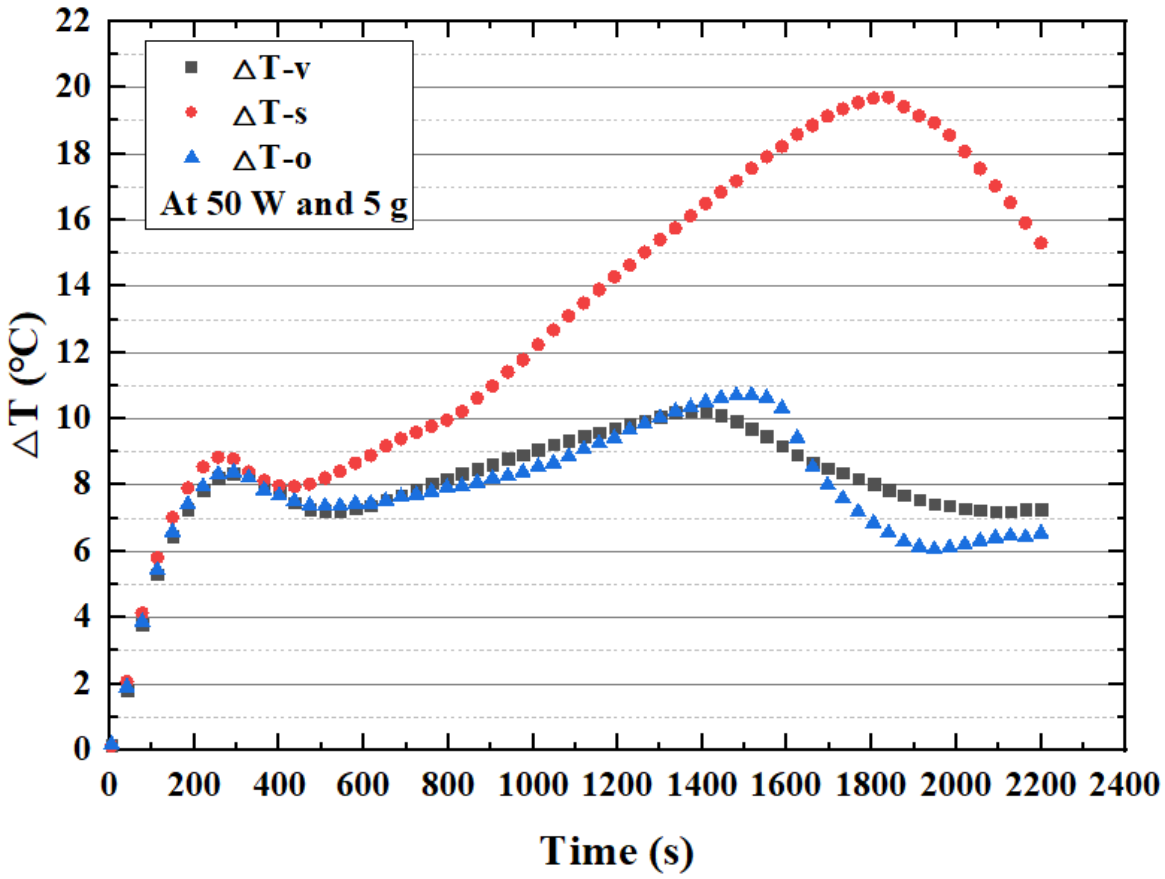

Fig. 10. Comparison of ΔT along different acceleration directions at 50 W and 5g.

For the purpose of comparison in a clear manner, the comparison of ΔT along acceleration direction at four different heating power of 40 W, 45 W, 50 W and 55 W is illustrated in Fig. 11.

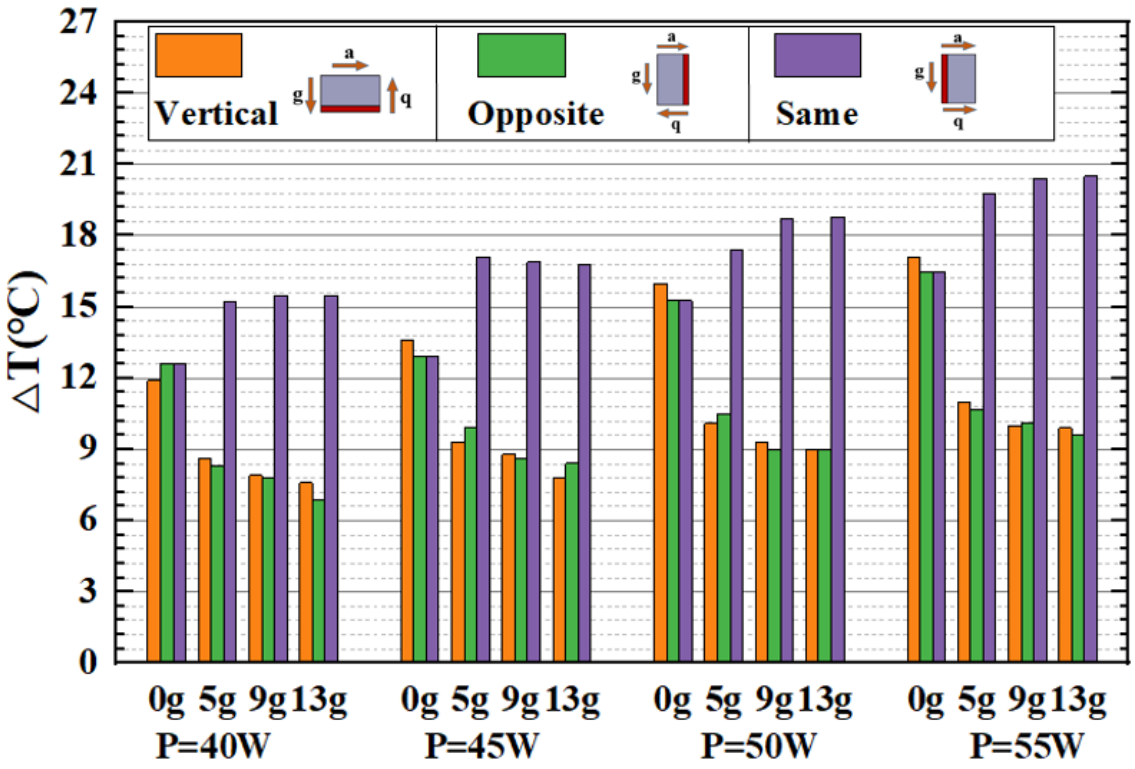

Fig. 11. The effects of acceleration direction on ΔT.

As can be seen from Fig. 11, at 0 g (ground), the effect of acceleration direction on ΔT does not show an obvious regularity. Under acceleration condition, there is no significant difference between ΔT-v and ΔT-o, but ΔT-s is significantly higher than ΔT-v and ΔT-o. For example, on the ground, ΔT-v, ΔT-o and ΔT-s at 40 W are 11.9 ℃, 12.6 ℃ and 12.6 ℃, respectively, while ΔT-v, ΔT-o and ΔT-s at 50 W are 16.0 ℃, 15.3 ℃ and 15.3 ℃, respectively. There is no regular effect of different acceleration directions on the thermal performance of PCESU under the two working conditions. Under acceleration conditions, at 40 W and 13 g, ΔT-v, ΔT-o and ΔT-s are 7.6 ℃, 6.9 ℃ and 15.5 ℃, respectively. In this case, ΔT-s is 7.9 ℃ and 8.6 ℃ higher than ΔT-v and ΔT-o, with the increase of 103.95% and 124.64%, respectively.

For all acceleration operating conditions, ΔT-v and ΔT-o are almost the same and the average difference is only 0.04 ℃. The average value of ΔT-s is 8.6 ℃ higher than that of ΔT-v, with an increase of 95.12%. It is suggested that the thermal performance along the same direction is significantly lower than that along vertical or opposite direction. Based on the analysis of t_m, the result shows that the PCESU could have the best thermal performance along vertical acceleration.

4.1.3. Analysis of experimental phenomena

According to phase change energy storage, there is a solid-liquid phase transition zone between melted and without n-eicosane during the melting process, which moves along the direction of heat flux with time. It is noted that, in the current study, the temperature distribution and liquid fraction inside the PCESU cannot be observed. Thus, in order to explore the physical mechanism, the working condition for acceleration magnitude of 5 g with heating power of 50 W along different acceleration direction is simulated with the proposed 2D simplified model. As shown in Fig. 12, the simulation results of liquid fraction are used as the schematic diagrams of n-eicosane melting process in PCESU for analysis.

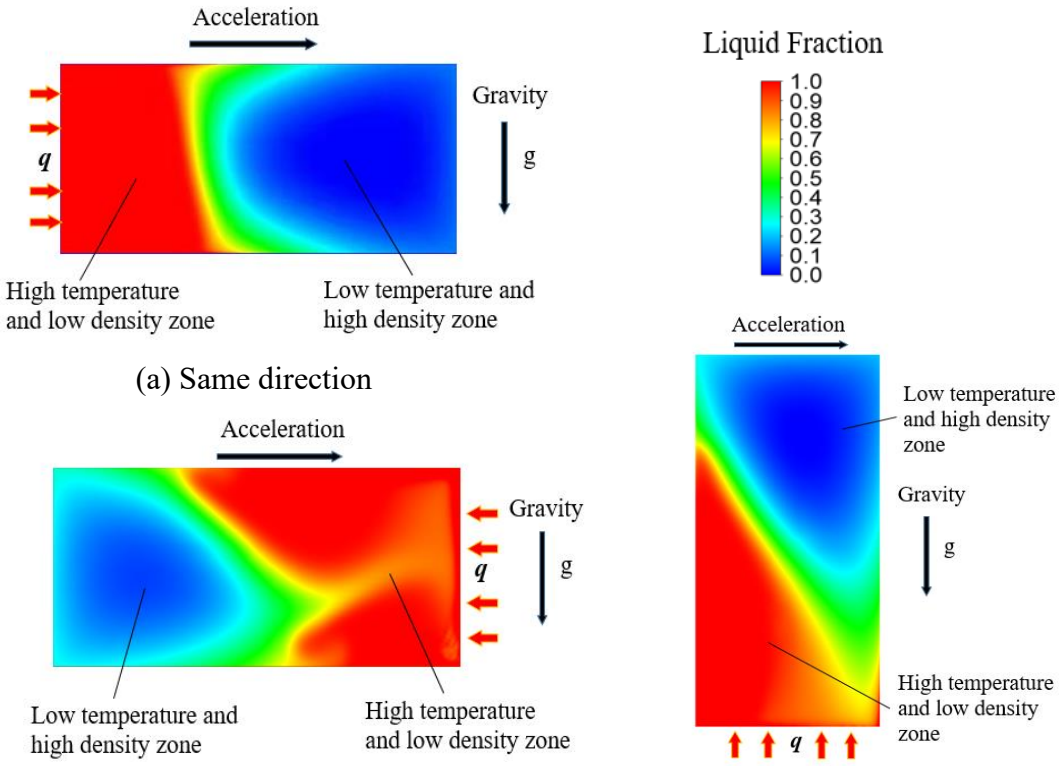

(a) Same direction

(b) Opposite direction

(c) Vertical direction

Fig. 12. Schematic diagram of n-eicosane melting process in PCESU in different acceleration directions: (a) same direction, (b) opposite direction and (c) vertical direction.

Since the copper foam is always being solid state during the melting process, the acceleration direction has almost no effect on its thermal performance. For the n-eicosane melting process in PCESU, the main reason for different results achieved could be the different natural convection caused by the buoyancy. The temperature distribution is uneven along the heat flux direction. For example, at 40 W, 5 g and along same direction, the temperature of layer A, B, C, D at melting time 2000 s are 38.0 ℃, 38.4 ℃, 42.9 ℃, 48.6 ℃ and 51.8 ℃, respectively. It can be seen from Fig. 12 that if considering the influence of temperature only, the n-eicosane from heat source to the phase change zone is liquid, and its temperature would gradually decrease. It is noted that the lower density of n-eicosane at high temperature and the higher density of n-eicosane at low temperature, the density of n-eicosane increases from the heat source to the phase change zone. When the temperature and density distribution are not uniform, the buoyancy will be generated in liquid n-eicosane, which will lead to a certain intensity of convection. This convection can enhance the heat transfer in PCESU.

According to the influence results of acceleration direction on t_m and ΔT, the main reasons could be explained as follows:

(i) as shown in Fig. 12(a), the heat flux direction is the same as acceleration direction, and the uniform temperature leads to an uneven density distribution of liquid n-eicosane in PCESU. The trend of buoyancy force caused by the temperature non-uniformity is to reduce the unevenness of the density, while the trend of acceleration action (n-eicosane with high density moving towards the acceleration direction) is to increase the unevenness. As a result, the acceleration effect along the same direction will suppress the convection caused by the uneven temperature. During the n-eicosane melting process, such suppression effect will lead to the increase of the thermal resistance and the final temperature difference of PCESU. Afterwards, the melting rate of n-eicosane slows

down and the temperature difference of PCESU.

(ii) along opposite direction, as demonstrated in Fig. 12(b), the effect of acceleration on the heat transfer is contrary to that along the same direction. The acceleration would enhance the convection and lead to the decrease of the thermal resistance and the final temperature difference of PCESU. Therefore, t_m-o and ΔT-o are smaller than t_m-s and ΔT-s during acceleration conditions.

(iii) as presented in Fig. 12(c), the heat flux direction is opposite to gravity direction along vertical direction. The combined effect of acceleration and gravity also enhances the convection caused by uneven temperature distribution and this enhancement is stronger than that along opposite direction. As a consequence, with the same acceleration magnitude and heating power, the t_m and ΔT along vertical direction are the smallest of that alone three direction.

4.2. Effects of acceleration magnitude on heat performance

4.2.1. Effects of acceleration magnitude on tm

According to the method described in Fig. 6, the effects of acceleration magnitude on t_m under different heating power along vertical, same and opposite directions are presented in Fig. 13.

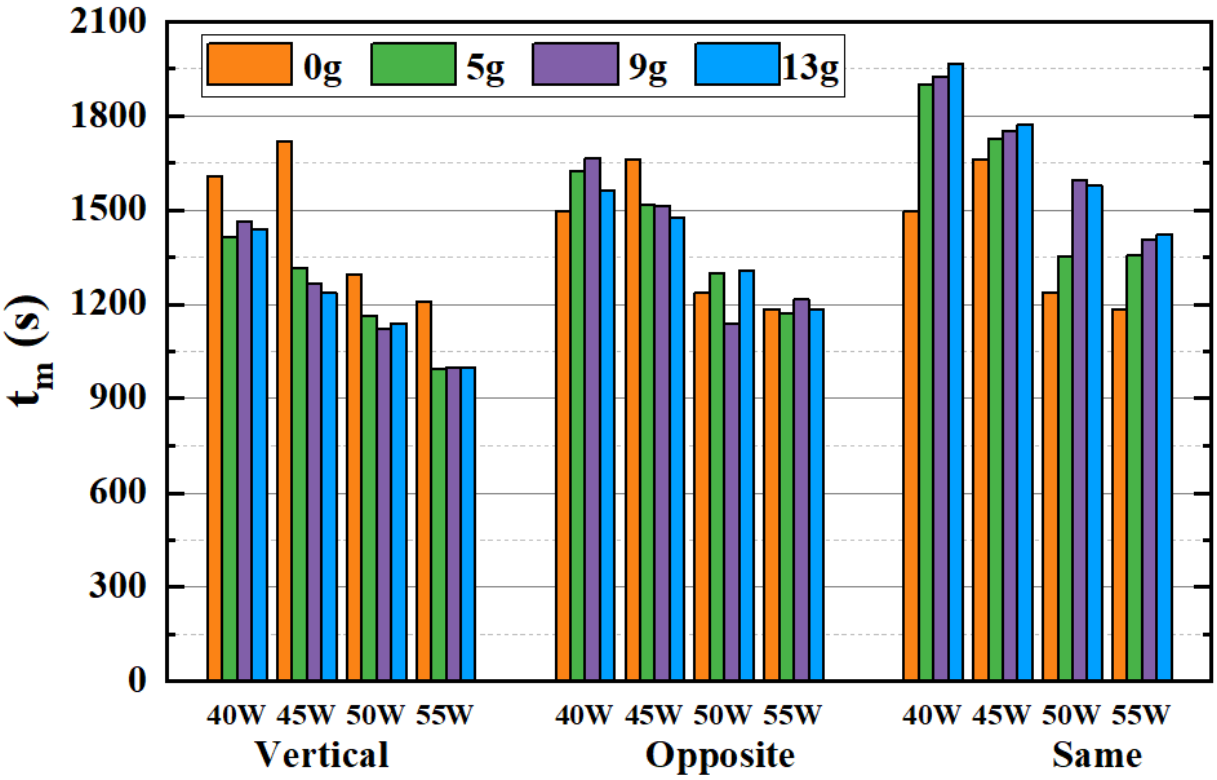

Fig. 13. The effects of acceleration magnitude on heat performance.

It can be seen from Fig. 13 that, along vertical direction, overall t_m decreases with the increase of the acceleration magnitude at different heating power. The reason could be due to the effect of acceleration direction on the thermal performance of PCESU. The combined effect of gravity acceleration and centrifugal acceleration can accelerate the melting of n-eicosane. The bigger the acceleration magnitude, the faster the paraffin melts. Although it is mentioned in section 4.1.3 that the acceleration could accelerate the melting process of PCESU along opposite direction, it can be seen from Fig. 13 that t_m does not show regular change with acceleration magnitude along this direction. The reason could be that the acceleration magnitude gradient set in the current experiment is too small. As a result, the effect is not obvious. Along the same direction, unlike the result shown along vertical direction, t_m increases with the increase of the acceleration magnitude

under a certain heating power. According to the analysis of the acceleration direction on n-eicosane melting process in section 4.1.3, the acceleration would suppress the convection of the liquid n-eicosane. And the suppression effect increases with the increase of the acceleration magnitude.

4.2.2. Effects of acceleration magnitude on ΔT

Fig. 14 shows the comparison of ΔT at heating power of 50 W along vertical direction at different acceleration magnitudes. From Fig. 14, it can be seen that ΔT has the same tendency as that in Fig. 10. ΔT gradually increases with time and is almost the same at different acceleration magnitudes before the paraffin starts to melt. Then it continues to increase gradually after a slight decrease. At 0 g, the ΔT becomes significantly larger compared with that for other acceleration magnitudes. In the acceleration environment, the difference of ΔT between different acceleration magnitudes is small. When the paraffin is completely melted, all of ΔT begins to decrease and the ΔT at 0 g is still obvious bigger than that of others.

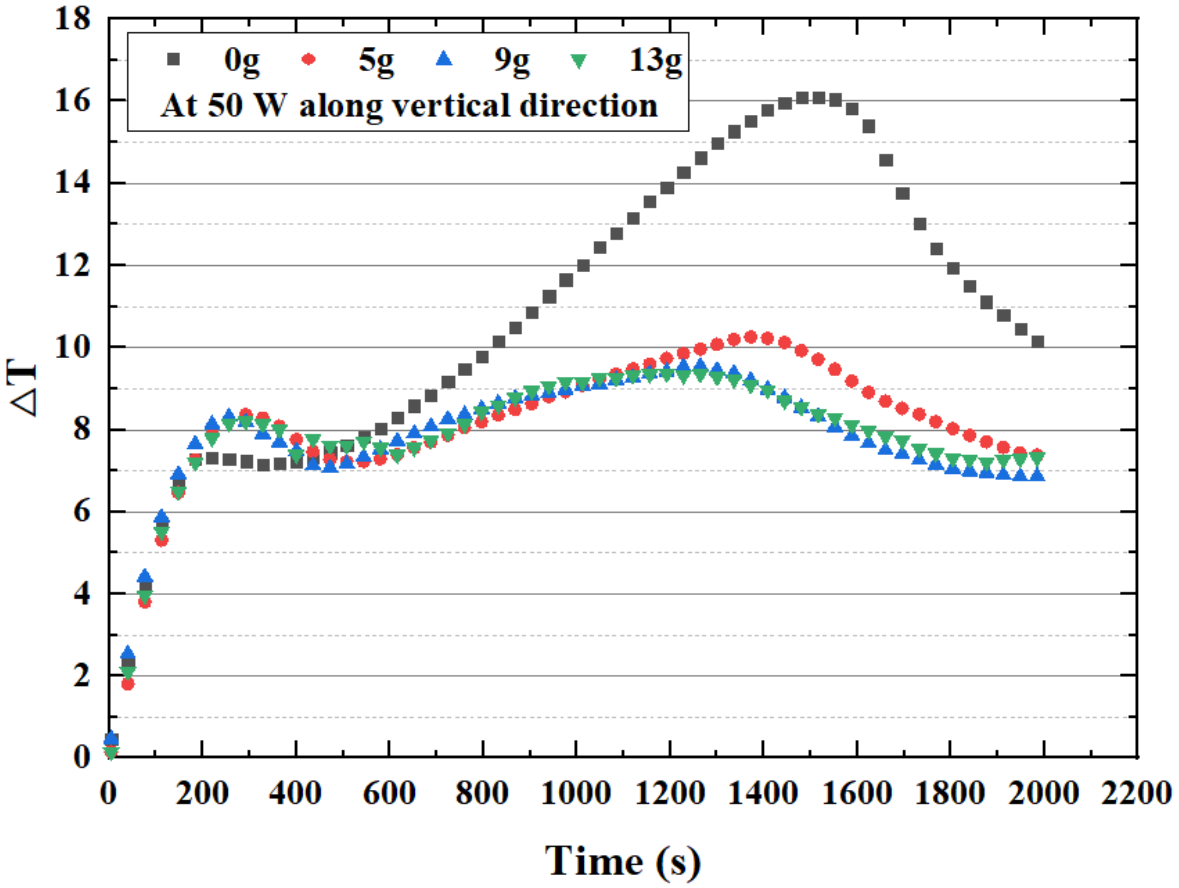

Fig. 14. Comparison of ΔT with different acceleration magnitudes at 50 W along vertical direction

According to the method described in Fig. 6, the effects of acceleration magnitude on ΔT at four different heating powers along vertical, same and opposite directions are plotted in Fig. 15.

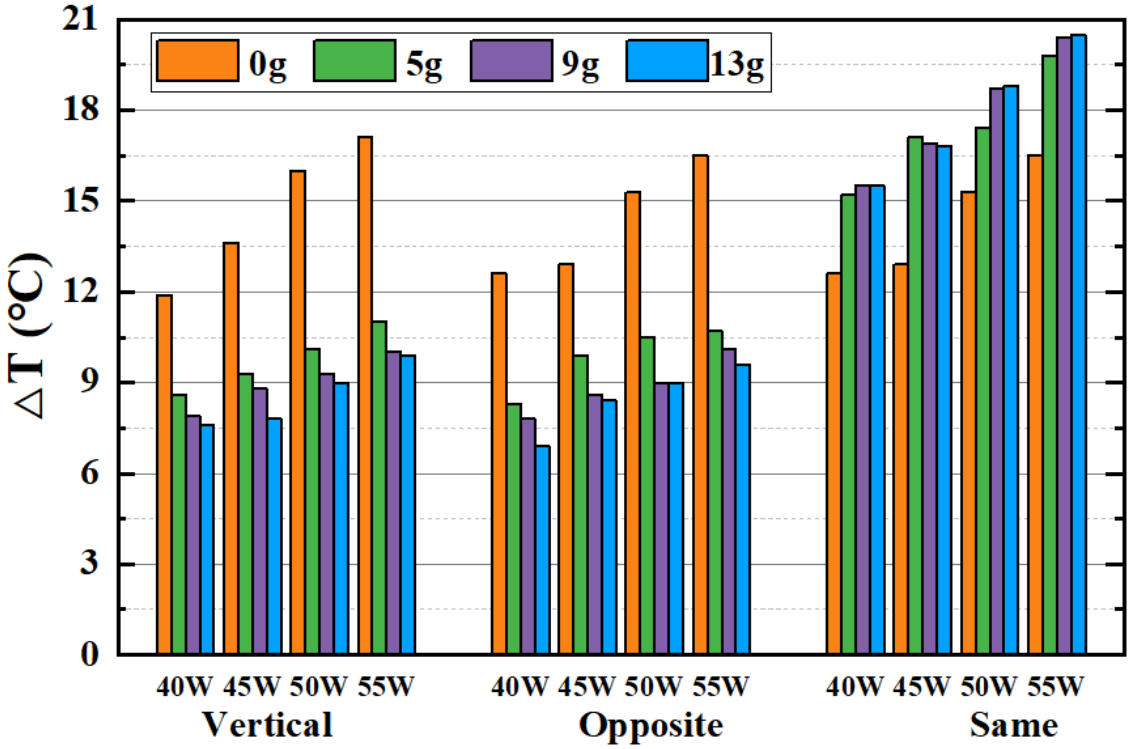

Fig. 15. The effects of acceleration magnitude on heat performance.

Fig. 15 indicates clearly that ΔT decreases with the increase of the acceleration magnitude under a certain heating power along vertical direction. Similar to the effect of acceleration direction on t_m, acceleration magnitude could enhance the natural convection in liquid n-eicosane along vertical direction. This enhancement could decrease the internal thermal resistance of PCESU and it increases with the increase of the acceleration magnitude. Along opposite direction and under certain heating power, although the acceleration magnitude has almost no obvious influence on t_m, ΔT decreases with the increase of the acceleration magnitude remarkably. As described in section 4.1.3, acceleration along opposite direction would reduce the thermal resistance in PCESU. This reduction effect could become greater as the acceleration magnitude increases, which could lead to the decrease of ΔT. Under the operating condition of same direction, ΔT generally increases with the increase of the acceleration magnitude for a certain heating power. As explained in section 4.1.3, the acceleration at same direction could lead to the increase of the thermal resistance of PCESU. Therefore, ΔT increases with the increase of the acceleration magnitude.

It is worth noting that t_m and ΔT have a larger change rate when the acceleration magnitude changes from static state (0 g) to 5 g. For example, along vertical direction, the average value of ΔT decreases by 4.9 ℃ from 0 g to 5 g with a decrease of 32.97 %. However, it only decreases by 0.8 ℃ and 0.4 ℃ when the acceleration magnitude changing from 5 g to 9 g and 9 g to 13 g, with the decreases of 7.81 % and 4.85 %, respectively. This could be explained by the fact that there is an initial "destroying" effect on the original flow field in liquid n-eicosane when the acceleration magnitude changed from 0 g to 5 g. Therefore, the change rate of t_m or ΔT is greater.

The above analysis illustrates that the acceleration magnitude has obvious influence on the thermal performance of PCUSE. The acceleration magnitude would have a contrary effect with different acceleration direction. It is important to take the acceleration direction into account when comparing the effect of acceleration magnitude.

4.3. *Effects of heating power on heat performance*

4.3.1. *Effects of heating power on tm*

Fig. 16 presents the comparisons of t_m at four different heating powers, i.e. 40 W, 45 W, 50 W and 55 W. It can be seen that t_m generally decreases with the increase of the heating power along certain acceleration direction and acceleration magnitude. For all the working conditions, the maximum value of t_m is 1966 s at 40 W and 13 g along the same direction. And the minimum value of t_m is 997 s at 55 W and 13 g along vertical direction. In general, t_m is negatively correlated to the heating power. It can be concluded that the higher the heat flux flows through the PCESU, the faster the n-eicosane melt and the smaller t_m.

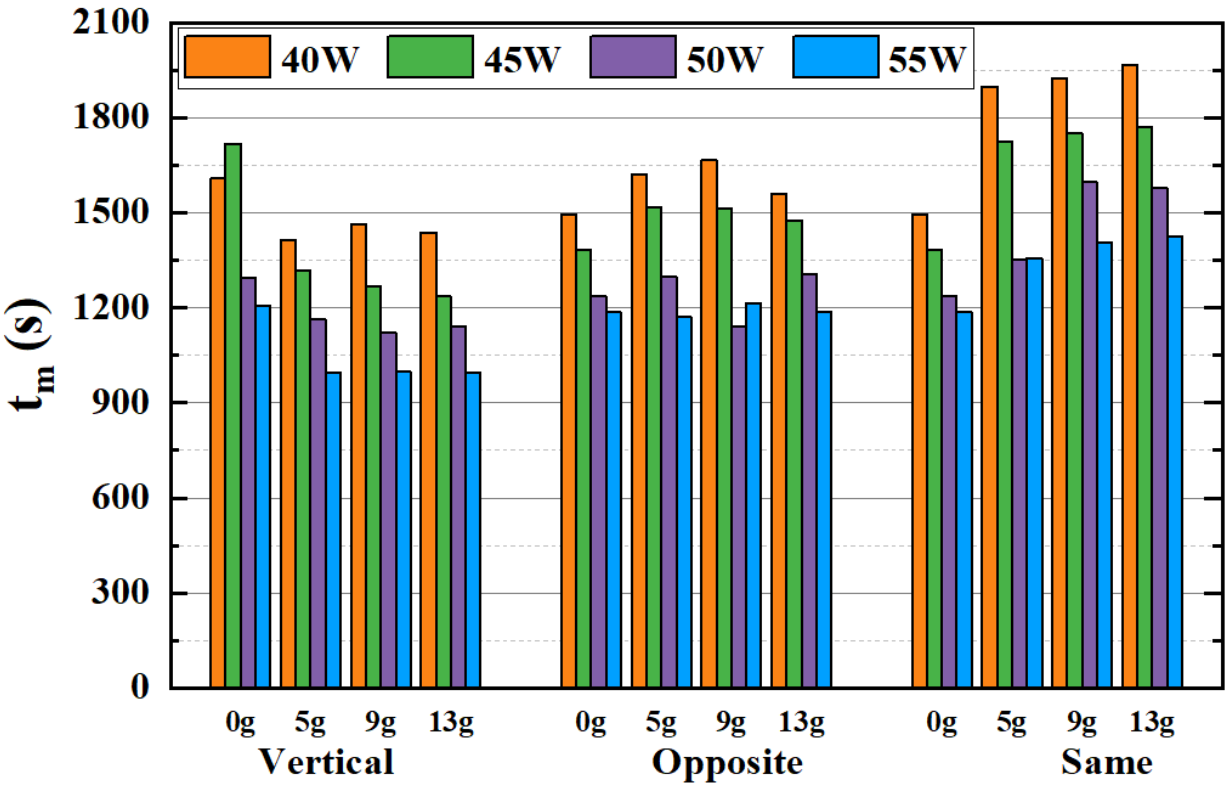

Fig. 16. The effects of heating power on t_m.

4.3.2. *Effects of heating power on* ΔT

Fig. 17 presents the comparisons of ΔT at four different heating powers. It can be found from Fig. 17 that ΔT increases with the increase of the heating power. For all the working conditions, the maximum ΔT is 20.5 ℃ at 55 W and 13g along the same direction, and the minimum ΔT is 6.9 ℃ at 40 W and 13g along opposite direction. In general, ΔT is positively correlated to the heating power. From the Fourier`s law of heat conduction:

$$q = -\lambda \frac{dT}{dx} \tag{6}$$

where λ presents thermal conductivity. It can be pointed that, when the acceleration and the heat flux direction are constant, only the heat flux q and the temperature gradient dT/dx are different. The higher the heat flux, the larger the temperature gradient. Therefore, ΔT increases with the increase of the heating power when it increases from 40 W to 55 W.

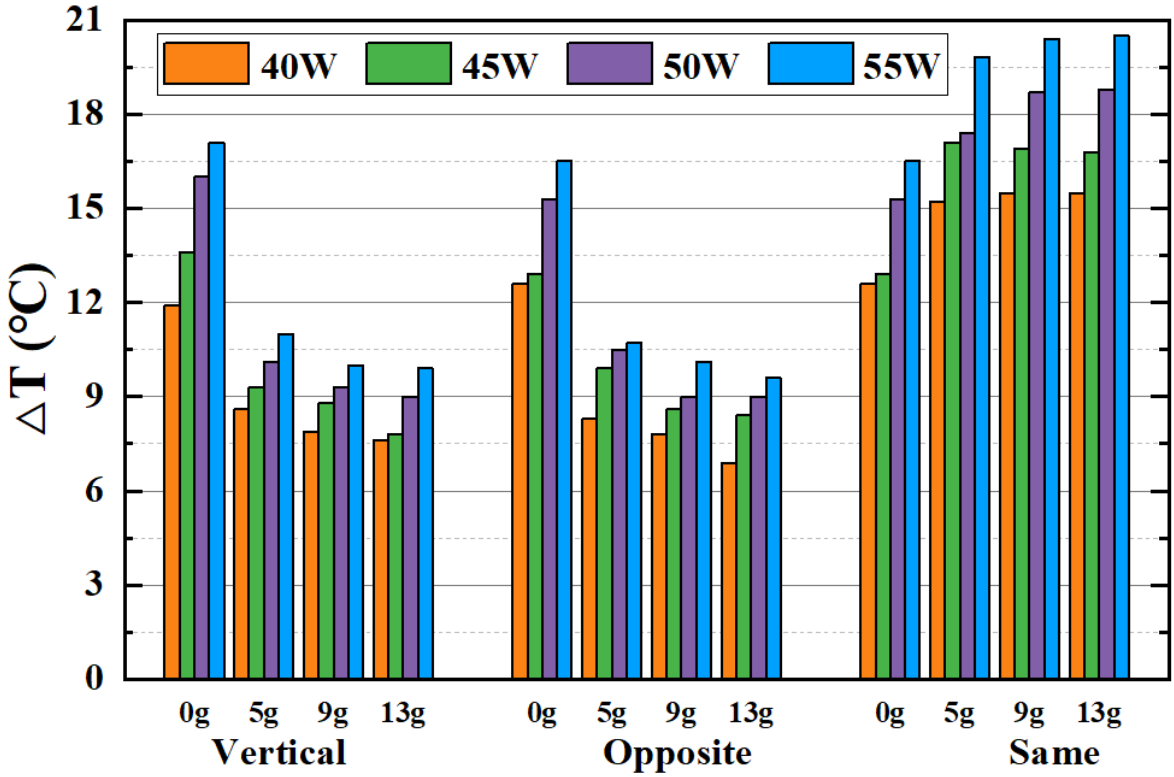

Fig. 17. The effects of heating power on ΔT.

5. Conclusions

A composite PCESU composed of copper foam (porosity of 97.2%), n-eicosane paraffin, and copper fins (thickness of 0.8 mm) was fabricated. The effects of several control parameters such as heating power, centrifugal acceleration magnitudes and directions on the thermal performance of PCESU was analyzed in a systematic manner. A 2D simplified simulation was carried to further reveal the physical mechanism of the thermal performance of PCESU. The results obtained in this study can be concluded as follows:

(1) The acceleration direction has a significant effect on the thermal performance of PCESU. The acceleration effects along vertical and opposite direction could improve the thermal performance of PCESU. While it shows a contrary effect along the same direction. Under acceleration conditions, t_m-s> t_m-o > t_m-v, and ΔT-v are almost the same with ΔT-o, but ΔT-s is significantly higher than ΔT-v and ΔT-o. The average values of t_m-o and t_m-s are 15.19% and 37.10% longer than that of t_m-v, and ΔT-s is 95.12% higher than that of ΔT-v.

(2) The effects of the acceleration magnitude on the thermal performance of PCESU depend on the acceleration direction. t_m and ΔT decreases with the increase of the acceleration magnitude along vertical direction and increases with that along the same direction. In addition, ΔT and t_m have a larger change rate from 0 g to 5 g. The average value of ΔT along vertical direction decreases 32.97 % from 0 g to 5 g and only 7.81 % and 4.85 % from 5 g to 9 g and 9 g to 13 g.

(3) The heating power has significant effects on t_m and ΔT. In general, t_m and ΔT are negatively and positively correlated to heating power, respectively. For all cases, the minimum value of t_m is 997 s at 55 W and 13 g along vertical direction. And the minimum value of ΔT is 6.9 ℃ at 40 W and 13 g along opposite direction.

(4) The acceleration along both vertical and opposite direction can enhance the natural convection of the melted n-eicosane in PCESU, and reduce the resistance of PCESU. It is a contrary effect along same direction. The bigger the acceleration magnitude, the stronger the acceleration effect. Moreover, along vertical direction, the combined effect of acceleration and gravity have a stronger enhancement than that along opposite direction.

In conclusion, when using PCESU under acceleration condition, the heat flux direction received by the energy storage unit should be vertical to acceleration direction as far as possible. This would contribute to shorten the melting time of the energy storage unit and reduce the temperature of the electronic components.

Acknowledgement

The authors acknowledge the financial supports from Joint innovation fund of First Academy and University (CALT201504) and Science Foundation for Distinguished Young Scholars 2020-JCJQ-ZQ-042. The authors would also like to thank the financial support from the internal funding of University of Hertfordshire, UK.

Reference

[1] Ling Z, Zhang Z, Shi G, et al. Review on thermal management systems using phase change materials for electronic components, Li-ion batteries and photovoltaic modules. Renewable and Sustainable Energy Reviews, 2014, 31: 427-438.

[2] Sahoo SK, Das MK, Rath P. Application of TCE-PCM based heat sinks for cooling of electronic components: A review. Renewable and Sustainable Energy Reviews, 2016, 59: 550-582.

[3] Khan Z, Khan Z, Ghafoor A. A review of performance enhancement of PCM based latent heat storage system within the context of materials, thermal stability and compatibility. Energy Conversion and Management, 2016, 115(5):132-158.

[4] Nazir H, Batool M, Osorio FJB, Isaza-Ruiz M, Xu XH, Vignarooban K, et al. Recent developments in phase change materials for energy storage applications: A review. International Journal of Heat and Mass Transfer 2019; 129:491-523.

[5] Samer K, Johnson MB, Kheirabadi AC, Groulx D, White MA. A comprehensive study of properties of paraffin phase change materials for solar thermal energy storage and thermal management applications. Energy 2018; 162: 1169-1182.

[6] Drissi S, Ling TC, Mo KB. Thermal efficiency and durability performances of paraffinic phase change materials with enhanced thermal conductivity–A review. Thermochimica acta 2019; 673: 198-210.

[7] Zhang P, Meng ZN, Zhu H, Wang YL, Peng SP. Melting heat transfer characteristics of a composite phase change material fabricated by paraffin and metal foam. Applied Energy 2017; 185: 1971-1983.

[8] Wang CH, Lin T, Li N, Zheng HP. Heat transfer enhancement of phase change composite material: Copper foam/paraffin. Renewable Energy 2016; 96:960-965.

[9] Zheng HP, Wang CH, Liu QM, Tian ZX, Fan XB. Thermal performance of copper foam/paraffin composite phase change material. Energy Conversion and Management 2018; 157: 372-381.

[10] Yao Y, Wu H, Liu Z. Direct simulation of interstitial heat transfer coefficient between paraffin and high porosity open-cell metal foam. Journal of Heat Transfer, 2018, 140(3).

[11] Sardari P T, Grant D, Giddings D, et al. Composite metal foam/PCM energy store design for dwelling space air heating. Energy Conversion and Management, 2019, 201: 112151.

[12] Buonomo B, Celik H, Ercole D, et al. Numerical study on latent thermal energy storage

systems with aluminum foam in local thermal equilibrium. Applied Thermal Engineering, 2019, 159: 113980.
[13] Ghahremannezhad A, Xu H, Salimpour M R, et al. Thermal performance analysis of phase change materials (PCMs) embedded in gradient porous metal foams. Applied Thermal Engineering, 2020, 179: 115731.
[14] Iasiello M, Mameli M, Filippeschi S, et al. Metal foam/PCM melting evolution analysis: Orientation and morphology effects. Applied Thermal Engineering, 2021, 187: 116572.
[15] Yao Y, Wu H. Thermal transport process of metal foam/paraffin composite (MFPC) with solid-liquid phase change: An experimental study. Applied Thermal Engineering, 2020, 179: 115668.
[16] Yao YP, Wu HY, Liu ZY. A new prediction model for the effective thermal conductivity of high porosity open-cell metal foams. International Journal of Thermal Sciences 2015; 97: 56-67.
[17] Bai X, Nakayama A. Quick estimate of effective thermal conductivity for fluid-saturated metal frame and prismatic cellular structures. Applied Thermal Engineering, 2019, 160:114011.
[18] Ashraf MJ, Ali HM, Usman H, Arshad A. Experimental passive electronics cooling: Parametric investigation of pin-fin geometries and efficient phase change materials. International Journal of Heat and Mass Transfer 2017; 115: 251-263.
[19] Wang ZW, Zhang HY, Xia X. Experimental investigation on the thermal behavior of cylindrical battery with composite paraffin and fin structure. International Journal of Heat and Mass Transfer 2017; 109: 958-970.
[20] Hussein A, Abd-Elhady MS, El-Sheikh MN, El-Metwally HT. Improving Heat Transfer Through ParaffinWax, by Using Fins and Metallic Strips. Arabian Journal for Science and Engineering 2018; 43:4433–4441.
[21] Ali HM, Arshad A, Jabbal M, Verdin PG. Thermal management of electronics devices with PCMs filled pin-fin heat sinks: A comparison. International Journal of Heat and Mass Transfer 2018; 117: 1199-1204.
[22] Ping P, Peng R, Kong D, et al. Investigation on thermal management performance of PCM-fin structure for Li-ion battery module in high-temperature environment. Energy conversion and management, 2018, 176: 131-146.
[23] Qureshi Z A, Ali H M, Khushnood S. Recent advances on thermal conductivity enhancement of phase change materials for energy storage system: a review. International Journal of Heat and Mass Transfer, 2018, 127: 838-856.
[24] Xu C, Xu S, Eticha R D. Experimental investigation of thermal performance for pulsating flow in a microchannel heat sink filled with PCM (paraffin/CNT composite). Energy Conversion and Management, 2021, 236: 114071.
[25] Zhang X, Zhu C, Fang G. Preparation and thermal properties of n-eicosane/nano-SiO2/expanded graphite composite phase-change material for thermal energy storage. Materials Chemistry and Physics, 2020, 240: 122178.
[26] Praveen B, Suresh S, Pethurajan V. Heat transfer performance of graphene nano-platelets laden micro-encapsulated PCM with polymer shell for thermal energy storage based heat sink. Applied Thermal Engineering, 2019, 156: 237-249.
[27] Raj C R, Suresh S, Vasudevan S, et al. Thermal performance of nano-enriched form-stable PCM implanted in a pin finned wall-less heat sink for thermal management application. Energy conversion and management, 2020, 226: 113466.
[28] Singh R P, Sze J Y, Kaushik S C, et al. Thermal performance enhancement of eutectic PCM laden with functionalised graphene nanoplatelets for an efficient solar absorption cooling storage system. Journal of Energy Storage, 2021, 33: 102092.
[29] Ramakrishnan S, Wang X, Sanjayan J, et al. Heat transfer performance enhancement of paraffin/expanded perlite phase change composites with graphene nano-platelets. Energy

Procedia, 2017, 105: 4866-4871.
[30] Ramakrishnan S, Wang X, Sanjayan J, et al. Assessing the feasibility of integrating form-stable phase change material composites with cementitious composites and prevention of PCM leakage. Materials Letters, 2017, 192: 88-91.
[31] Chamkha A , Veismoradi A , Ghalambaz M , et al. Phase change heat transfer in an L-Shape heatsink occupied with paraffin-copper metal foam. Applied Thermal Engineering, 2020, 177:115493.
[32] Hu X, Gong X. Experimental and numerical investigation on thermal performance enhancement of phase change material embedding porous metal structure with cubic cell. Applied Thermal Engineering, 2020, 175: 115337.
[33] Zhang H, Li X, Liu L, et al. Experimental investigation on paraffin melting in high porosity copper foam under centrifugal accelerations. Applied Thermal Engineering, 2020, 178: 115504.
[34] Yang K, Liu K, Wang J. Pore-scale numerical simulation of convection heat transfer in high porosity open-cell metal foam under rotating conditions. Applied Thermal Engineering, 2021: 117168.
[35] Wu G, Chen S, Zeng S. Effects of mechanical vibration on melting behaviour of phase change material during charging process. Applied Thermal Engineering, 2021, 192: 116914.